frontiers
in Astronomy and
Space Sciences

TYPE Methods
PUBLISHED 23 October 2026
DOI 10.3389/fspas.2026.1986629

Check for updates

OPEN ACCESS

EDITED BY
Martin Volwerk,
Austrian Academy of Sciences, Austria

REVIEWED BY
Costel Munteanu,
Institute of Space Science, Romania
Neal Hurlburt,
Lockheed Martin Space Systems,
United States

*CORRESPONDENCE
Vicki Toy-Edens,
vicki.toy-edens@jhuapl.edu

RECEIVED 02 September 2026
REVISED 29 September 2026
ACCEPTED 01 October 2026
PUBLISHED 23 October 2026

CITATION
Toy-Edens V, Mo W, Raptis S, Bell NC, Dąbrowska M, Eschweiler T, Ford RA, Gonano V, Gorokhov ACRB, Leal Quesada JM, Luperchio AM and Pasqua A (2026) Shock Detectives: classifying MMS observations of Earth's magnetosheath via citizen science. *Front. Astron. Space Sci.* 13:1986629. doi: 10.3389/fspas.2026.1986629

COPYRIGHT
© 2026 Toy-Edens, Mo, Raptis, Bell, Dąbrowska, Eschweiler, Ford, Gonano, Gorokhov, Leal Quesada, Luperchio and Pasqua. This is an open-access article distributed under the terms of the Creative Commons Attribution License (CC BY). The use, distribution or reproduction in other forums is permitted, provided the original author(s) and the copyright owner(s) are credited and that the original publication in this journal is cited, in accordance with accepted academic practice. No use, distribution or reproduction is permitted which does not comply with these terms.

Shock Detectives: classifying MMS observations of Earth's magnetosheath via citizen science

Vicki Toy-Edens[1]*, Wenli Mo[1], Savvas Raptis[1], Nathan C. Bell[2], Magdalena Dąbrowska[2], Thorsten Eschweiler[2], Rachel A. Ford[2], Virgilio Gonano[2], Andrey C. R. B. Gorokhov[2], Jose Manuel Leal Quesada[2], Adeline M. Luperchio[2] and Antonio Pasqua[2]

[1]Johns Hopkins University Applied Physics Laboratory, Laurel, MD, United States, [2]Shock Detectives Citizen Scientist, Laurel, MD, United States

We present a dataset of 35,483 unique 1 minute periods (~591 h) of quasi-perpendicular and quasi-parallel magnetosheath MMS classifications manually reviewed with the help of citizen scientists. This dataset spans a variety of representative solar wind conditions sampled over the course of 8 years of data on the dayside. We identify 7,697 high likelihood quasi-parallel magnetosheath minute intervals and an additional 2,315 moderate likelihood quasi-parallel intervals. Within this dataset, we also identify 2,677 temporal transitions between quasi-perpendicular and quasi-parallel magnetosheath at 1-min resolution. This rich dataset can be used to perform statistical studies of these two populations and to train machine learning models.

KEYWORDS
citizen science, classification, dataset, magnetosheath, MMS, quasi-parallel, quasi-perpendicular

1 Introduction

As supersonic solar wind interacts with the Earth's magnetosphere, it forms a collisionless bow shock. Downstream of that shock, the turbulent, shocked, and highly variable plasma found in the region is called magnetosheath. This region is essential for understanding fundamental processes such as magnetic reconnection, turbulence, and energy transfer throughout the magnetosphere system. The properties of these shocks depend on the direction of the interplanetary magnetic field (IMF) relative to the shock normal, producing two distinct shock geometries and subsequent magnetosheath regions. These regimes are referred to as quasi-perpendicular, when the IMF is oriented mostly perpendicular ($\theta_{Bn} \gtrsim 45°$) to the shock normal, and quasi-parallel, when the IMF is oriented mostly parallel ($\theta_{Bn} \lesssim 45°$) to the shock normal. The quasi-parallel magnetosheath is generally more turbulent than quasi-perpendicular magnetosheath leading to different instabilities, transient structures, and wave activity (Eastwood et al., 2018). Understanding the behavior of these two regimes is therefore important for studying collisionless shocks and physical processes that influence the solar wind-magnetosphere coupling.

Although quasi-perpendicular and quasi-parallel magnetosheath intervals can often be identified using bow shock models and upstream conditions or *in-situ* observed plasma and

magnetic field quantities (Raptis et al., 2020b; Karlsson et al., 2021; Svenningsson et al., 2025), there has not yet been a robust and easy to use algorithm capable of systematically classifying these regions at scale using the local information available. One challenge to basic methods that employ fixed rules or thresholds based on observed quantities (Koller et al., 2024) is the large variability in solar wind conditions. Standard approaches that rely on upstream solar wind measurements from OMNIweb or missions like ACE and Wind from the Lagrangian 1 (L1) point can also be inaccurate and unpredictable (Vokhmyanin et al., 2019; Walsh et al., 2019; Raptis et al., 2020a) due to spatial and temporal variability of the solar wind (Borovsky, 2018; Walsh et al., 2019; Burkholder et al., 2020) and the ambiguity in propagation time from L1 to Earth's bow shock (Mailyan et al., 2008; Case and Wild, 2012; O'Brien et al., 2023).

Quasi-perpendicular and quasi-parallel magnetosheath exhibit substantially different properties when measured with *in-situ* spacecraft (Formisano and Hedgecock, 1973; Gosling et al., 1978; Luhmann et al., 1986; Crooker et al., 1981; Anderson et al., 1994; Fuselier et al., 1994; Yordanova et al., 2020). This knowledge has motivated recent efforts to classify these regions directly from *in-situ* observations, rather than relying on model-based approaches, with considerable success. However, these efforts have been limited to narrow time intervals, applicable to only certain data products, or specific transient phenomena (high-speed jets) rather than the entire magnetosheath environment (Raptis et al., 2020b; a; Karlsson et al., 2021; Koller et al., 2024; Svenningsson et al., 2025). While these studies give credence to *in-situ* classification being superior to previous techniques, they highlight the difficulty of obtaining a well-classified dataset from a systematic effort to generate classifications across the whole magnetosheath environment and that extend to different missions. Another limitation is the large amount of *in-situ* observations of the magnetosheath that need to be classified.

In this work, we present a large manually labeled dataset of quasi-perpendicular and quasi-parallel magnetosheath from the Magnetospheric Multiscale (MMS; Burch et al., 2015) mission. The dataset spans a wide range of solar wind conditions and was categorized by citizen scientists through the Zooniverse platform. A dataset of this size can enable statistical studies of these two magnetosheath populations and supports the development and validation of future automated classification algorithms.

2 Materials and methods

2.1 Data

This work uses a list of classified magnetosheath intervals of 15 min or longer from Toy-Edens et al., 2024 for MMS1. Toy-Edens et al., 2024 applied an automated, unsupervised machine learning algorithm to 8 years (September 2015 to 31 January 2024) of dayside ($X_{GSE} > 0$) MMS Level 2 survey/fast data. Each minute was classified as one of four plasma regions: magnetosphere, magnetosheath, solar wind, or ion foreshock. The resulting list of intervals that each MMS probe stayed within a given plasma region for at least 15 min is publicly available on Zenodo (Toy-Edens, 2024). We additionally incorporate the magnetosheath jet intervals identified by Raptis et al., 2020b, who detected jets from May 2015 to June 2020 based on thresholding statistical plasma properties, in order to include disturbed magnetosheath intervals.

We use a sample of 35,483 unique 1 minute periods (~591 h) that is representative of the multidimensional range of solar wind and observational conditions, including variations in solar wind density, speed, mean local time, and year (Figure 1). We incorporate all Raptis et al., 2020b magnetosheath jets classified as quasi-parallel, quasi-perpendicular, or boundary jets into our sample (~15%–20% of our sample), with each jet centered within a 5-min interval. Another ~15%–20% of our sample consists of 5-min intervals shifted either 5 minutes before or after the jet (randomly chosen) to capture the surrounding quasi-parallel or quasi-perpendicular magnetosheath in the absence of a jet. The remaining intervals were randomly selected from the 15-min magnetosheath intervals identified by Toy-Edens et al., 2024, excluding intervals already included in the previously selected epochs. All intervals in the sample were manually reviewed by an expert to reject periods contaminated by solar wind or magnetospheric plasma. This review removed approximately 10% of the initial sample, primarily because we evaluated at the higher native temporal resolution of MMS rather than the 1-min resolution used by Toy-Edens, 2024.

For each interval, we use the survey Fast Plasma Investigation (FPI, Pollock et al., 2016) ion spectra and temperature data at native resolution of 4.5 s and Fluxgate Magnetometers (FGM, Torbert et al., 2014) magnetometer data at 62.5 ms. We also pull the OMNI (King and Papitashvili, 2005) high-resolution 1-min cadence proton density and plasma flow speed for the entire 5-min interval. We then calculate the average value of the OMNI data within each interval to provide a representative estimate of the upstream solar wind and IMF conditions.

2.2 Methods

Citizen scientists are volunteers from the public who contribute to scientific research. In our citizen science project[1], hosted through the Zooniverse platform, citizen scientists examine a three-panel figure (Figure 2) containing five consecutive 1-min intervals. For each interval, they classify the magnetosheath as: (1) either quasi-perpendicular or quasi-parallel and (2) mixed, containing distinct sections of both quasi-perpendicular and quasi-parallel within the interval, or unmixed. These classifications are collected through two distinct workflows applied to the same set of sample images (Figure 2).

Our methodology follows a similar approach as Svenningsson et al., 2025, which uses a combination of measurements of magnetic fluctuations, energetic ion flux, and ion temperature anisotropy. However, rather than applying fixed thresholds, we present citizen scientists with figures that display these quantities. The displayed measurements are: (1) ion spectrogram from FPI, (2) parallel and perpendicular ion temperatures from FPI, and (3) the magnetic fluctuation parameter

1 https://www.zooniverse.org/projects/vickitoyedens/shock-detectives

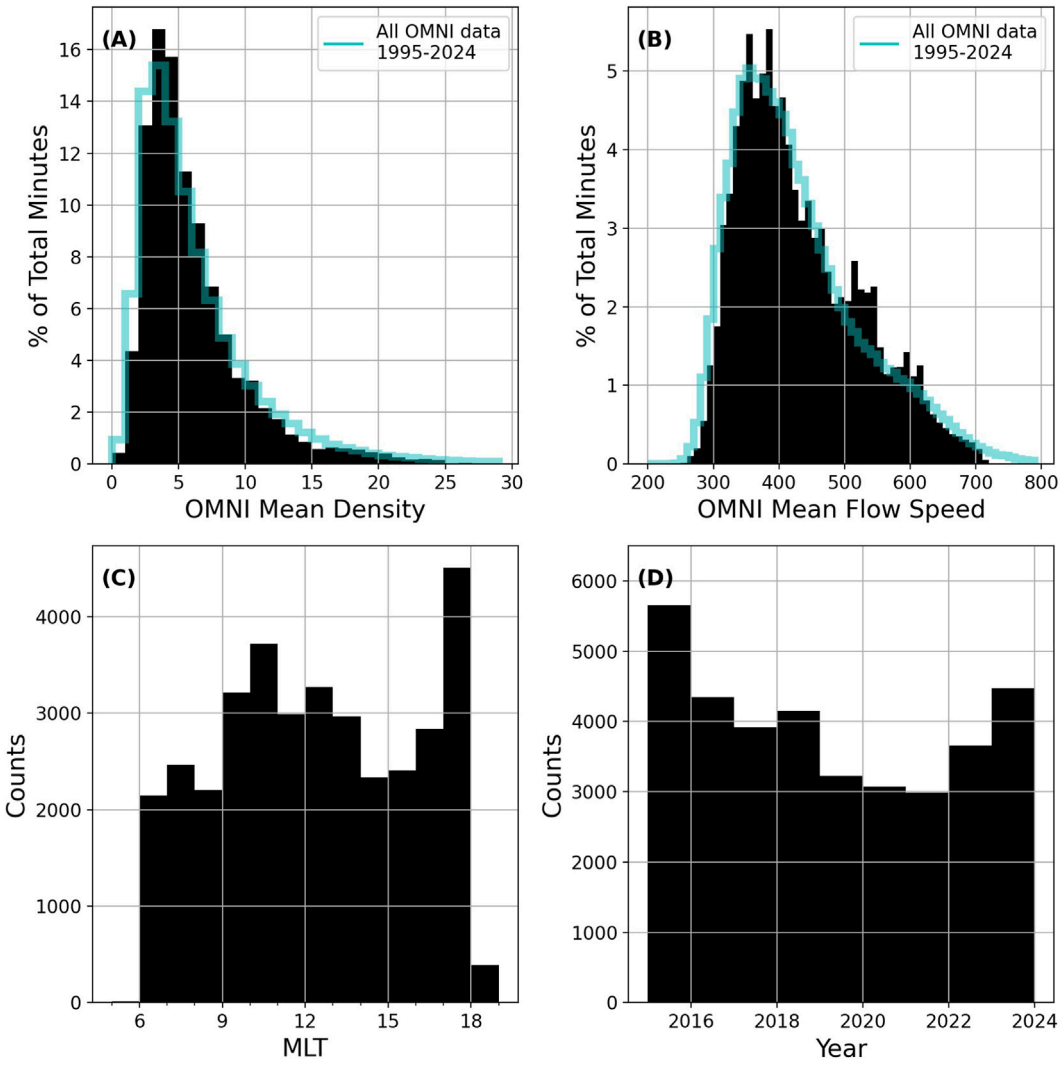


FIGURE 1
Distribution of total minutes in the sample that were shown to the citizen scientists as a function of **(A)** OMNI mean density, **(B)** OMNI mean flow speed, **(C)** mean local time, and **(D)** year. The cyan overlays in **(A)** and **(B)** show the corresponding OMNI distributions from 1995–2024.

used by Svenningsson et al., 2025 shown in Equation 1 from FGM.

$$\overline{\sigma_B} = \frac{\sqrt{\sigma_{30s}(B_x)^2 + \sigma_{30s}(B_y)^2 + \sigma_{30s}(B_z)^2}}{< B_{30s} >} \quad (1)$$

where $\sigma_{30s}(B_n)$ is the standard deviation of the magnetic field component over a 30 s window and $< B_{30s} >$ is the mean of the magnetic field magnitude over a 30 s window.

The tutorial provided to citizen scientists explains that quasi-parallel magnetosheath is more likely when: (1) the ion spectrogram exhibits enhanced high energy flux relative to low energy flux, (2) the parallel and perpendicular temperature coincide, and (3) $\overline{\sigma_B}$ is elevated. Conversely, quasi-perpendicular magnetosheath is generally characterized by comparatively weaker suprathermal ion flux, greater ion temperature anisotropy, and lower magnetic field variability. These signatures were treated as qualitative and complementary indicators rather than three independent binary criteria. Classifications were based on the overall pattern across all three measurements, allowing intervals to be classified as quasi-parallel or quasi-perpendicular even when one or more indicators were ambiguous or had competing signatures. When measurements did not fully agree, citizen scientists were encouraged to select the classification most strongly supported by the combined evidence. To guide classifications, we include a shaded gray band near the $\overline{\sigma_B}$ threshold. We shade between 0.1 and 0.3 whereas the Svenningsson et al., 2025 threshold is 0.29. Citizen scientists are then asked to identify which, if any, minutes in the 5 minute interval contain predominantly quasi-parallel magnetosheath in the quasi-parallel/quasi-perpendicular workflow. This workflow asked volunteers to select intervals while making sure the user interface was designed in a way to avoid interpreting as if all three quasi-parallel signatures need to be simultaneously satisfied. By avoiding strict threshold-based classifications, this approach allows the citizen scientists to incorporate more nuanced pattern recognition into their decision making. In the mixed workflow, citizen scientists are asked to identify which, if any, minutes in the

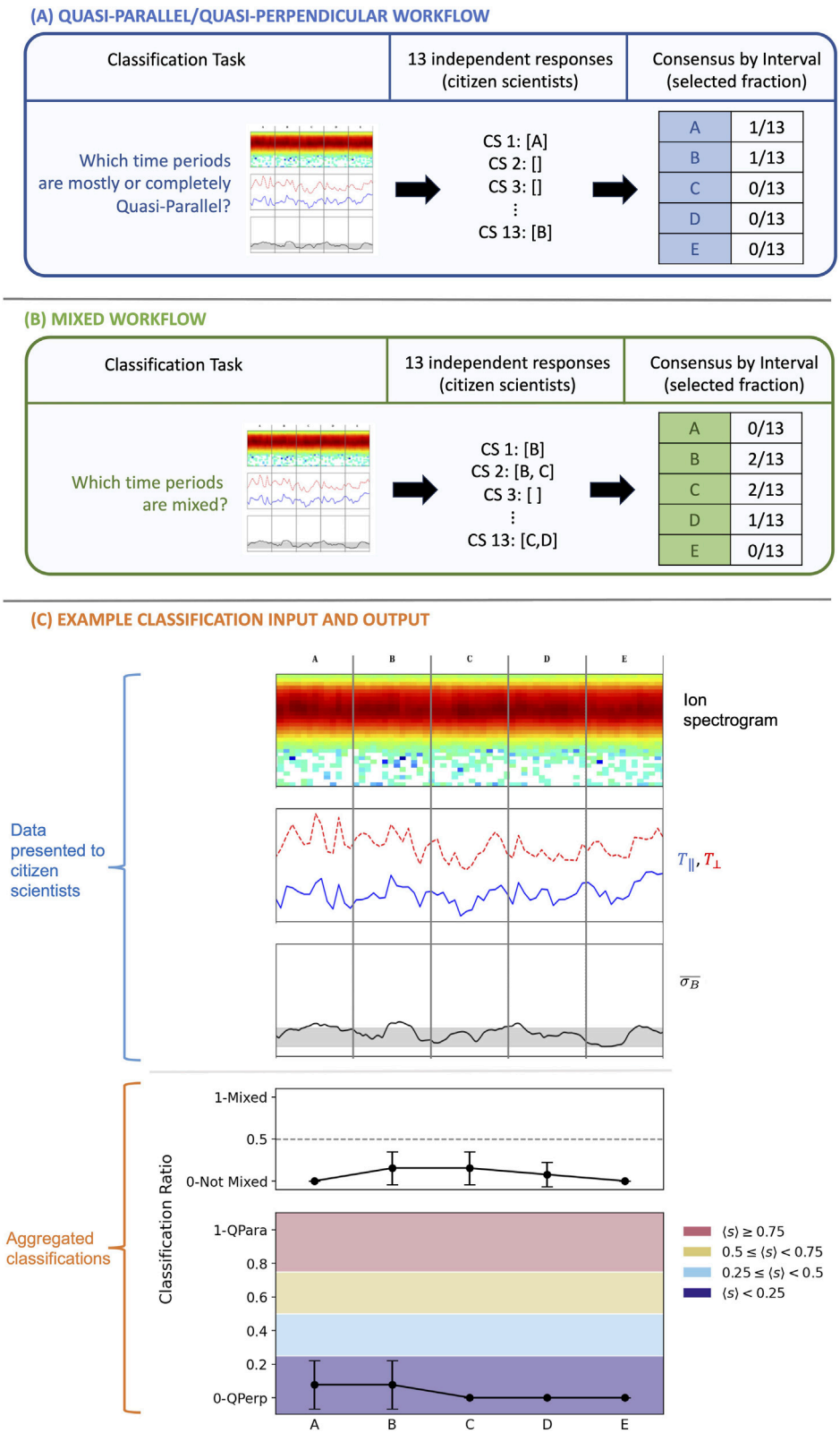


FIGURE 2
Overview of the two classification workflows and an example of the input and aggregated results. Citizen scientists classified five consecutive 1-min intervals as quasi-perpendicular/quasi-parallel and mixed/unmixed, with 13 independent responses collected per workflow. Panels **(A)** and **(B)** illustrate how responses were converted to interval-level classification fractions. In panel **(C)**, the upper three panels show the MMS data presented to volunteers: the FPI ion spectrogram, $T_{\parallel}$ and $T_{\perp}$ from FPI, and $\overline{\sigma_B}$ from FGM. The lower panels show the aggregated mixed and quasi-parallel classification fractions. The dashed horizontal line marks the 50% mixed threshold, the colored bands indicate quasi-parallel agreement ranges, and vertical dashed green lines mark identified transitions when present.

5 minute interval contain a temporal transition from quasi-parallel to quasi-perpendicular magnetosheath (or *vice versa*).

Each 1-min interval within a 5 minute sample receives 13 independent classifications (Figure 2) for each workflow. This number was chosen by visual inspection of classifications during a smaller 300 subject beta testing. While very simple intervals had full agreement with five independent classifications, extremely complex environments had several differing opinions and we require more classifications to get the "wisdom of the crowd." For each workflow, we compute the normalized classification score or consensus selected fraction, $\langle s \rangle$, across all citizen scientists (Figure 2) for each 1-min interval. For the quasi-parallel/quasi-perpendicular workflow a value of 0 indicates unanimous agreement that the interval is quasi-perpendicular and a value of 1 indicates unanimous agreement that the interval is quasi-parallel. Whereas, for the mixed workflow a value of 0 indicates unanimous agreement that the interval is unmixed and a value of 1 indicates unanimous agreement that the interval is mixed.

An example of the input (highlighted in blue) and the output (highlighted in orange) for a single 5 minute period is shown in Figure 2C from MMS1 for 2017–11–11 02:44–02:49 UTC. This example shows that the consensus from the citizen scientists is that all five 1-min periods are quasi-perpendicular (with high agreement) and unmixed. This example shows the utility of manual classification because the ion spectra is shifted to higher than typical energy bands.

The transitions between quasi-perpendicular and quasi-parallel classifications from the mixed workflow were more difficult to identify, leading to fewer flagged transition instances. Therefore, in addition to reporting intervals with high mixed-classification agreement, $\langle s \rangle \geq 0.5$, between citizen scientists, we use a combination of both workflows to identify and refine transitions. A transition is flagged when the absolute difference between neighboring classifications from the quasi-parallel/quasi-perpendicular workflow exceed 0.4, indicating a substantial change in classifications. This threshold was selected through visual inspection of the distribution of neighboring-classification differences. Because a potential transition lies between two adjacent 1-min intervals, we select the minute with the higher classification score, $\langle s \rangle$, from the mixed workflow. This indicates that the citizen scientists more strongly associated that minute with a temporal transition.

3 Results

The distribution of our 35,483 unique 1 minute periods (~591 h) are shown in Figures 3A,B and Table 1. From visual inspection, we identify four classification bins for the quasi-parallel/quasi-perpendicular workflow (< 0.25, [0.25, 0.5), [0.5, 0.75), ≥0.75). We report 10,012 (28.2% of all classifications) of quasi-parallel classifications using the 0.5 threshold and 7,697 (21.7% of all classifications) for the 0.25 threshold. This distribution is consistent with the statistical expectation we have from Parker spiral orientation at Earth's orbit, a point further discussed below. We similarly set a high threshold on the mixed workflow to identify high likelihood transition intervals using a threshold of ≥ 0.5 on the mixed workflow (2,190 or 6.2% of all classifications) and with our combined workflow method (1,248 or 3.5% of all classifications). The total number of unique transition intervals using either method is 2,677 or 7.5% of all classifications. This dataset is publicly available on Zenodo (Toy-Edens et al., 2026).

In order to evaluate the robustness of citizen scientist classifications, we incorporated 2,140 duplicate minutes. Each duplicate minute was classified by two to four sets of 13 citizen scientists, providing samples of classification variability; some citizen scientists may have contributed to more than one set. The distribution of disagreements for the normalized classification score from the minimum to maximum score differential for the primary workflow is shown in Figure 3C. Only 81 (3.7% of duplicate minutes) exceeded a difference of 0.25 which corresponds to jumping a full classification category. This indicates that our selection of 13 citizen scientist classifications per sample is robust to human subjectivity.

Examples of different types of classifications are shown in Figure 4. There are examples of very stable quasi-parallel and quasi-perpendicular magnetosheath alongside some rapid transitions. The citizen scientists picked up on these transitions even when there were competing signals of both types of magnetosheath. For instance, in Figure 4C, the parallel and perpendicular temperatures follow quasi-perpendicular characteristic pattern in time periods D and E but the citizen scientists were still in agreement that it was quasi-parallel magnetosheath. The identified transitions also align with changes between different types of magnetosheath.

We evaluate the distributions of the three parameters Svenningsson et al., 2025 used for thresholds as well as the parameters the citizen scientists were trained to identify (Figure 5): suprathermal ion flux, ion temperature anisotropy, and measured magnetic field variability. The suprathermal ion flux is measured by integrating the top three highest ion energy channels. Note that MMS changes the range of these energy channels through the lifetime of the mission so the energy range is not consistent. Svenningsson et al., 2025 notes that the suprathermal ion flux cannot be used reliably for FPI fast mode. For the remaining parameters, we label the Svenningsson et al., 2025 threshold with dashed black vertical lines. For the high likelihood quasi-perpendicular, $\langle s \rangle <$ 0.25, or high likelihood quasi-parallel, $\langle s \rangle \geq 0.75$, classifications, they align with the thresholds except there are distribution tails. However, for the lower likelihood classifications where there is some nuance given disagreement between citizen scientists, they do not fall exactly within the hard thresholds. This suggests that the citizen scientists may have been able to make more nuanced judgment calls by incorporating contextual information. For example, they may have recognized when the suprathermal ion flux shifted toward the upper end of the MMS ion energy range in fast mode (Figure 2), as expected under fast solar wind conditions (Koller et al., 2024), and used the surrounding magnetosheath structure as an indication of local variability.

Quasi-parallel classifications skew toward the dawn side and quasi-perpendicular toward the dusk side (Figure 6). This is the statistically expected pattern since the Parker spiral maps the IMF to roughly 45° from the Sun-Earth line, so on average the field connects more nearly along the shock normal on the dawn flank (quasi-parallel) and closer to perpendicular on dusk. The scatter, however, is very large. Any single interval is therefore unlikely to sit at its statistically preferred location, as clearly demonstrated by Figure 6.

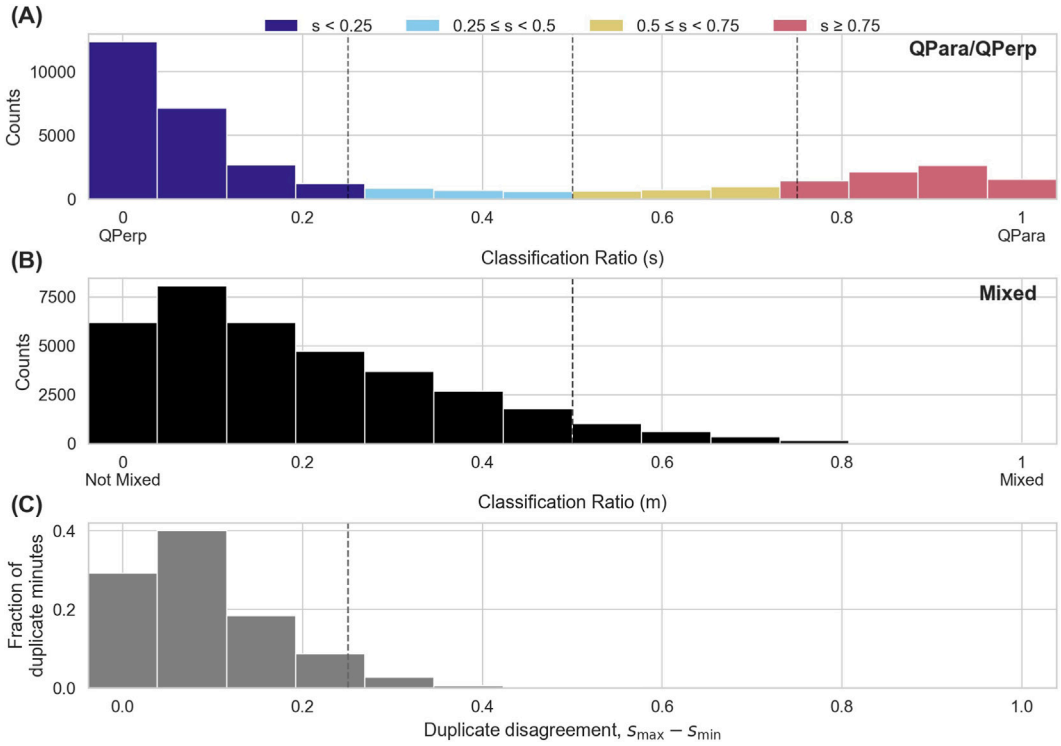


FIGURE 3
Distributions of classification scores and duplicate-sample disagreement. Panels **(A)** and **(B)** show the classification-score distributions from the quasi-parallel/quasi-perpendicular and mixed workflows, respectively; dashed vertical lines mark the adopted classification thresholds. Panel **(C)** shows the distribution of the difference between the maximum and minimum mean quasi-parallel/quasi-perpendicular scores, $s_{max} - s_{min}$, for duplicate 1-min intervals. Each duplicate interval was independently evaluated by two to four groups of 13 citizen scientists, although individual volunteers may have contributed to more than one group, to assess the robustness of the classifications.

TABLE 1 **Distribution of sample classifications.**

Quasi-parallel/perpendicular category	Count	Percent
< 0.25 (High likelihood QPerp)	23,366	65.8%
[0.25, 0.5)	2,105	5.9%
[0.5, 0.75)	2,315	6.5%
≥0.75 (High likelihood QPara)	7,697	21.7%
Mixed category	**Count**	**Percent**
Transition (0.5 threshold)	2,190	6.2%
Transition (combined workflow method)	1,248	3.5%
Unique transitions (both methods)	2,677	7.5%

4 Discussion

With this large and diverse dataset of quasi-perpendicular and quasi-parallel magnetosheath classifications, detailed statistical studies can be performed to compare these two magnetosheath populations. For instance (Kajdič et al., 2021; Turc et al., 2022), have shown that foreshock waves are transmitted downstream of the shock, suggesting that the quasi-parallel magnetosheath should contain a significantly larger population of ultra-low frequency (ULF) waves than the quasi-perpendicular magnetosheath. This distinction is important because ULF waves can significantly influence the magnetospheric system (Hartinger et al., 2013; Wang et al., 2020; Liu et al., 2025; Liu et al.,2026). The large statistical sample provided by this dataset can therefore be used to further investigate these processes and connect upstream foreshock conditions to magnetospheric activity. Similar studies can be conducted on the transmission and prevalence of other upstream transient phenomena (Kajdič et al., 2024), such as magnetic holes (Karlsson et al., 2022), (spontaneous) hot flow anomalies (Omidi et al., 2016; Raptis et al., 2025; Zhou et al., 2026), foreshock compressive boundaries (Sibeck et al., 2021; Kajdič et al., 2026), foreshock compressive structures (Karlsson et al., 2015; Raptis et al., 2022; Bai et al., 2025; Xirogiannopoulou et al., 2026), and turbulent structures (Trotta et al., 2022), among others.

Another direct application of this dataset is to evaluate the prevalence, occurrence, and properties of transient processes within each magnetosheath region. While previous efforts have examined the relationship between different magnetosheath environments and magnetosheath jets (Raptis et al., 2020b), a

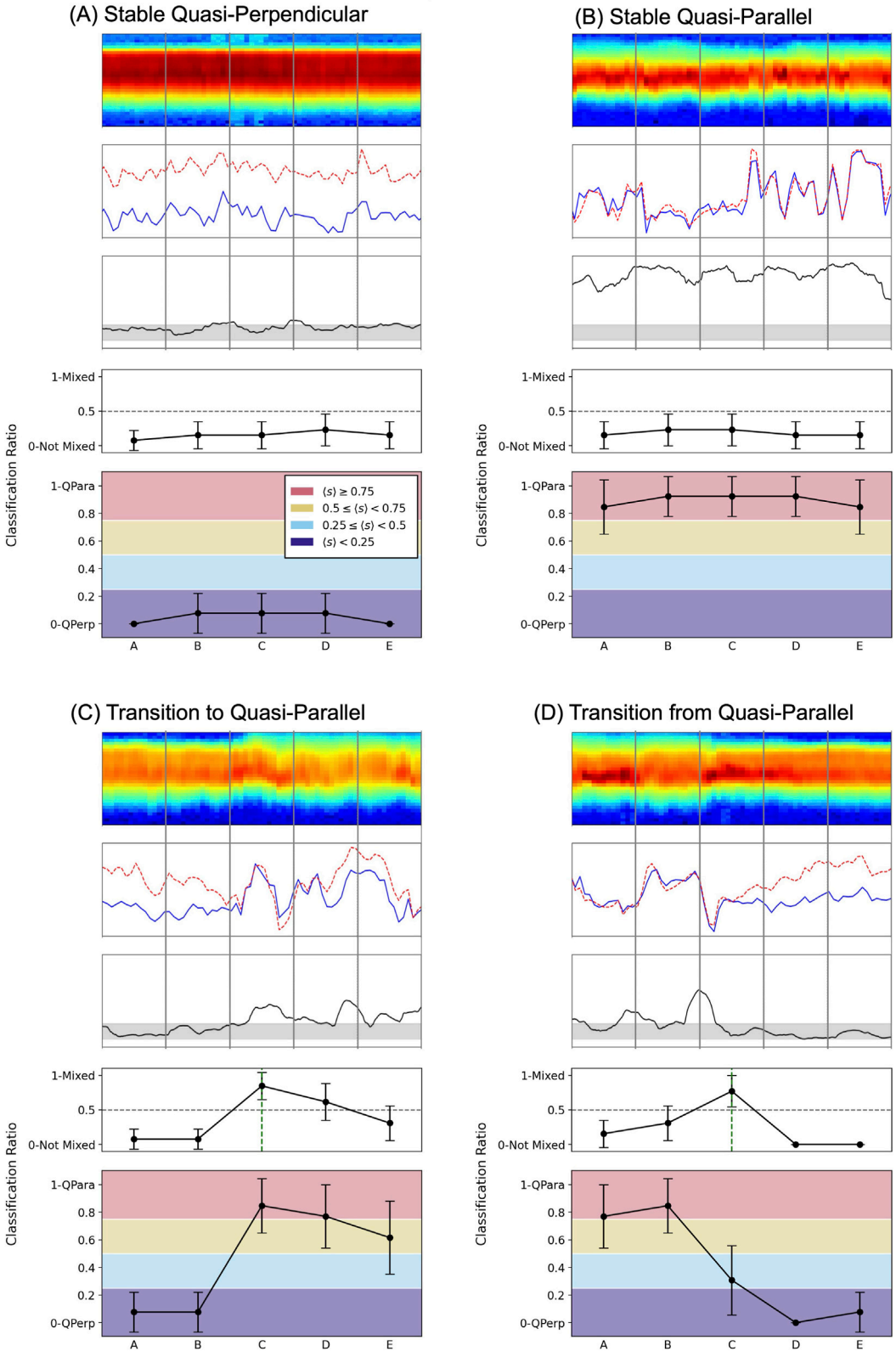


FIGURE 4
Four representative 5 minute samples. **(A)** An example from 2020–02–28 22:26–22:31 UTC that was classified as stable quasi-perpendicular magnetosheath. **(B)** An example from 2018–04–26 09:24–09:29 UTC that was classified as stable quasi-parallel magnetosheath. **(C)** An example from 2015–11–05 09:26–09:31 UTC that was classified as quasi-perpendicular magnetosheath for 2 minutes then transitioning within the 3rd minute to quasi-parallel magnetosheath. Note that the 3rd and 4th minute are flagged as transitions (the 3rd minute identified by our multi-workflow method). **(D)** An example from 2015–11–05 11:09–11:14 UTC that was classified as quasi-parallel magnetosheath for 2 minutes then transitioning within the 3rd minute to quasi-perpendicular magnetosheath. Note that the 3rd minute is flagged as a transition (identified by both the multi-workflow method and the 50% threshold).

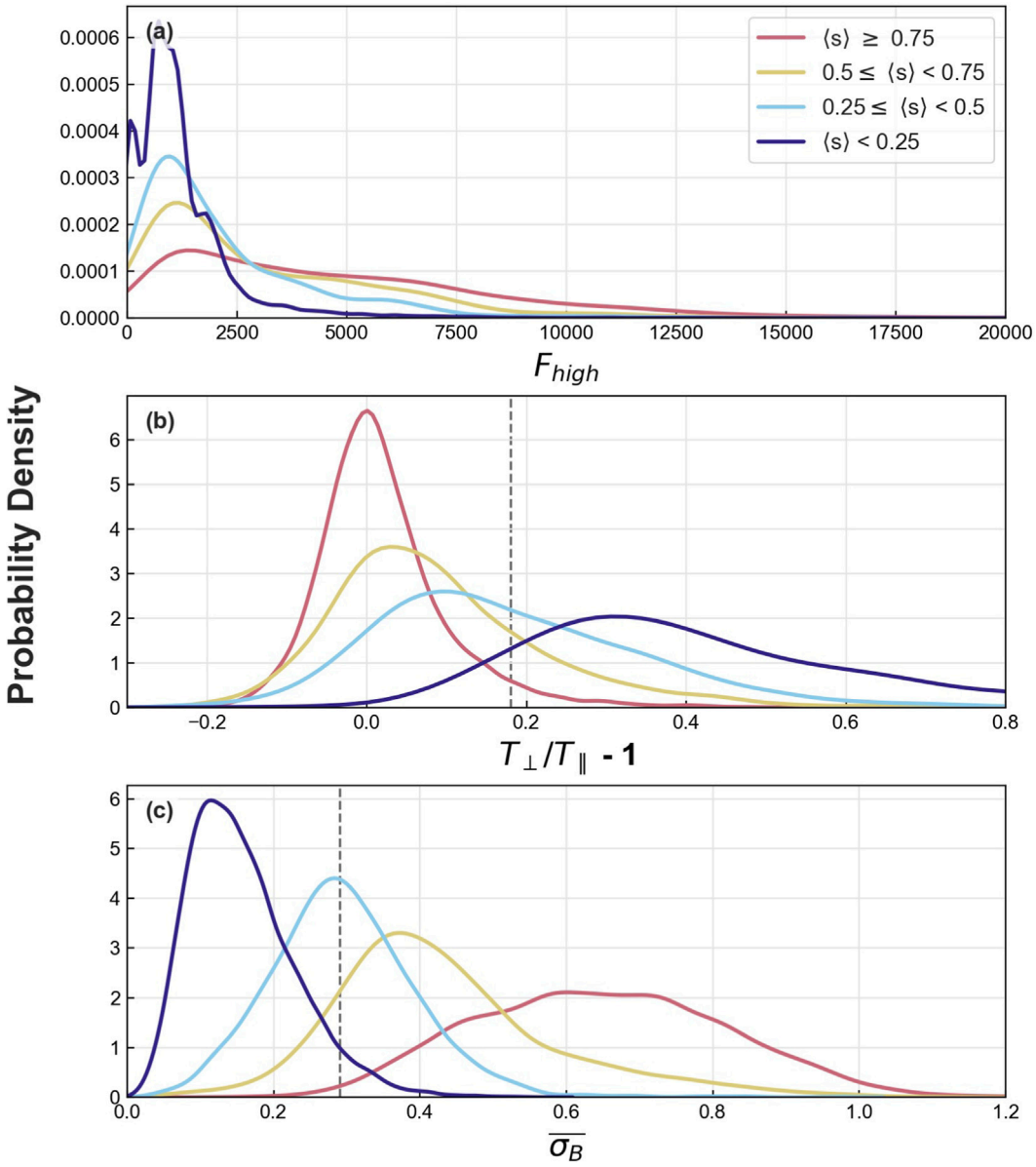


FIGURE 5
Distribution of the three Svenningsson et al., 2025 parameters. **(A)** Measurement of suprathermal ion flux (integrated flux of top three ion energy bands), **(B)** ion temperature anisotropy, and **(C)** measured magnetic field variability. Consistent with qualitative signatures, the high-likelihood quasi-parallel and quasi-perpendicular populations tend to occupy opposite portions of the energetic particle, temperature anisotropy, and magnetic variability distributions, although substantial overlap remains.

statistically robust connection between magnetosheath regions and transient processes has yet to be established. This is particularly important for jets appearing near the transition between the two magnetosheath environments. Although several hypotheses have been proposed regarding their nature (Archer and Horbury, 2013; Raptis et al., 2020b; Sibeck et al., 2021), their occurrence rates and characteristic properties have not yet been established, in part because of the lack of a sufficiently comprehensive and well-separated dataset. Addressing these questions is especially important because such processes have been found to be ubiquitous at planetary shocks and can influence magnetospheric dynamics, while their generation mechanisms, occurrence rates, and properties remain open questions (Plaschke et al., 2018; Krämer et al., 2024). Our team plans to address this topic in a follow-up article.

Beyond jets, other transient processes and localized effects have yet to be systematically studied using a clean and well-separated magnetosheath dataset. Such separation is particularly valuable for studies of phenomena such as turbulence evolution in the magnetosheath (Bandyopadhyay et al., 2020; Pecora et al., 2026), where mixing plasma populations associated with quasi-parallel and quasi-perpendicular geometries can violate stationarity assumptions and introduce statistical artifacts, including Simpson's Paradox (Blyth, 1972). Another prominent application of this dataset is

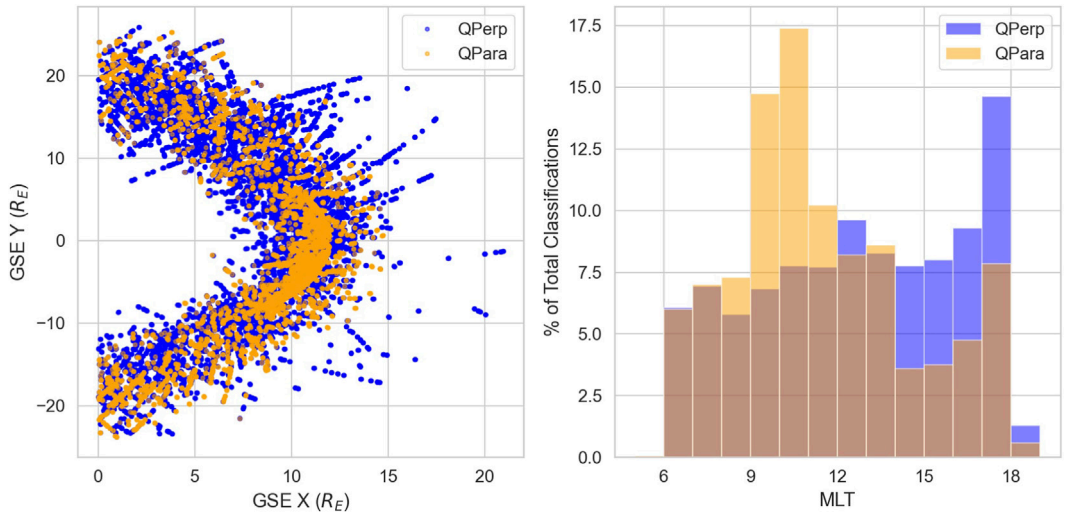


FIGURE 6
Distribution of (left) quasi-parallel and quasi-perpendicular classifications in the GSE X-Y plane in Earth radii and (right) mean local time. Blue indicates quasi-perpendicular magnetosheath, orange indicates quasi-parallel magnetosheath, and brown indicates the overlap between the two distributions. Note that there is a skew of quasi-parallel classifications on the dawn side, and a duskside preference for quasi-perpendicular classifications; consistent with the expected Parker spiral interplanetary magnetic field orientation.

to statistically evaluate whether near-bow-shock crossings are associated with quasi-parallel or quasi-perpendicular geometries when using bow shock modeling and single or multi spacecraft shock analysis techniques. Comparison with this classified dataset can provide an important diagnostic for assessing whether plasma conditions measured upstream of Earth's bow shock can be assumed to remain physically relevant to downstream observations, and over what spatial and temporal scales this assumption remains valid. Such efforts are important for the broader community because future missions such as ESA's Plasma Observatory (Retinò et al., 2022) aim to investigate multi-scale plasma processes. Establishing the extent of spatiotemporal relationships across these boundaries will therefore be necessary to refine mission design and science objectives.

In the future, we also aim to train a machine learning model to reproduce this classification and apply it to MMS observations beyond the end of the present training sample, i.e., after 2024. This will be particularly useful for expanding the statistical sample over time, potentially covering multiple solar cycles and a wider range of upstream conditions. Finally, another promising application is to investigate whether such a trained model can be used for transfer learning (Toy-Edens et al., 2025) across missions with observations similar to MMS, such as THEMIS (Angelopoulos, 2008) and ESA's Cluster (Escoubet et al., 2001). Ultimately, this approach could be extended across the Solar System to environments such as Mars using MAVEN observations (Jakosky et al., 2015), where recent studies have identified both distinct differences and notable similarities relative to Earth's magnetosheath and foreshock environments (Mohammed-Amin et al., 2025; Zhang et al., 2025).

Data availability statement

The datasets presented in this study can be found in online repositories. The names of the repository/repositories and accession number(s) can be found below: https://zenodo.org/records/22210989 (DOI: 10.5281/zenodo.22210988).

Author contributions

VT-E: Conceptualization, Data curation, Formal Analysis, Investigation, Methodology, Software, Validation, Visualization, Writing – original draft, Writing – review and editing. WM: Conceptualization, Data curation, Methodology, Software, Validation, Visualization, Writing – review and editing. SR: Conceptualization, Validation, Writing – original draft, Writing – review and editing. NB: Data curation, Writing – review and editing. MD: Data curation, Writing – review and editing. TE: Data curation, Writing – review and editing. RF: Data curation, Writing – review and editing. VG: Data curation, Writing – review and editing. AG: Data curation, Writing – review and editing. JL: Data curation, Writing – review and editing. AL: Data curation, Writing – review and editing. AP: Data curation, Writing – review and editing.

Funding

The author(s) declared that financial support was received for this work and/or its publication. This work was funded by grant 80NSSC25K0153 from the NASA CSSFP program.

Acknowledgments

This publication uses data generated via the Zooniverse.org platform, development of which is funded by generous support, including from the National Science Foundation, NASA, the Institute of Museum and Library Services, UKRI, a Global Impact Award from Google, and the Alfred P. Sloan Foundation. We thank the citizen scientists who contributed to the Shock Detectives classifications through Zooniverse (complete list of contributors at https://www.zooniverse.org/projects/vickitoyedens/shock-detectives/talk/7265/4105991). We utilized HelioCloud platform (Thomas et al., 2022) for part of our computation and thank the HelioCloud team for their support.

Conflict of interest

The author(s) declared that this work was conducted in the absence of any commercial or financial relationships that could be construed as a potential conflict of interest.

Generative AI statement

The author(s) declared that generative AI was used in the creation of this manuscript. to assist with grammar, wording, and clarity during manuscript preparation. All Generative AI suggestions were reviewed and approved by the authors.

Any alternative text (alt text) provided alongside figures in this article has been generated by Frontiers with the support of artificial intelligence and reasonable efforts have been made to ensure accuracy, including review by the authors wherever possible. If you identify any issues, please contact us.

Publisher's note

All claims expressed in this article are solely those of the authors and do not necessarily represent those of their affiliated organizations, or those of the publisher, the editors and the reviewers. Any product that may be evaluated in this article, or claim that may be made by its manufacturer, is not guaranteed or endorsed by the publisher.

References

Anderson, B. J., Fuselier, S. A., Gary, S. P., and Denton, R. E. (1994). Magnetic spectral signatures in the earth's magnetosheath and plasma depletion layer. *J. Geophys. Res. Space Phys.* 99, 5877–5891. doi: 10.1029/93ja02827

Angelopoulos, V. (2008). The THEMIS mission. *Space Sci. Rev.* 141, 5–34. doi: 10.1007/s11214-008-9336-1

Archer, M., and Horbury, T. (2013). Magnetosheath dynamic pressure enhancements: occurrence and typical properties. *Ann. geophysicae Copernic. Publ. Göttingen, Ger.* 31, 319–331. doi: 10.5194/angeo-31-319-2013

Bai, S.-C., Guo, R., Shi, Q., Tian, A., Zhang, H., Qin, S., et al. (2025). Statistical analysis of the short large-amplitude magnetic structures: evolution and ion resonance. *Geophys. Res. Lett.* 52, e2025GL116547. doi: 10.1029/2025gl116547

Bandyopadhyay, R., Matthaeus, W. H., Parashar, T. N., Yang, Y., Chasapis, A., Giles, B. L., et al. (2020). Statistics of kinetic dissipation in the earth's magnetosheath: MMS observations. *Phys. Rev. Lett.* 124, 255101. doi: 10.1103/physrevlett.124.255101

Blyth, C. R. (1972). On Simpson's paradox and the sure-thing principle. *J. Am. Stat. Assoc.* 67, 364–366. doi: 10.1080/01621459.1972.10482387

Borovsky, J. E. (2018). The spatial structure of the oncoming solar wind at earth and the shortcomings of a solar-wind monitor at L1. *J. Atmos. Solar-Terrestrial Phys.* 177, 2–11. doi: 10.1016/j.jastp.2017.03.014

Burch, J. L., Moore, T. E., Torbert, R. B., and Giles, B. L. (2015). Magnetospheric Multiscale overview and science objectives. *Space Sci. Rev.* 199, 5–21. doi: 10.1007/s11214-015-0164-9

Burkholder, B. L., Nykyri, K., and Ma, X. (2020). Use of the L1 constellation as a multispacecraft Solar Wind Monitor. *J. Geophys. Res. Space Phys.* 125, e2020JA027978. doi: 10.1029/2020ja027978

Case, N., and Wild, J. (2012). A statistical comparison of solar wind propagation delays derived from multispacecraft techniques. *J. Geophys. Res. Space Phys.* 117. doi: 10.1029/2011ja016946

Crooker, N., Eastman, T., Frank, L., Smith, E., and Russell, C. (1981). Energetic magnetosheath ions and the interplanetary magnetic field orientation. *J. Geophys. Res. Space Phys.* 86, 4455–4460. doi: 10.1029/ja086ia06p04455

Eastwood, J. P., Mistry, R., Phan, T. D., Schwartz, S. J., Ergun, R. E., Drake, J. F., et al. (2018). Guide field reconnection: exhaust structure and heating. *Geophys. Res. Lett.* 45, 4569–4577. doi: 10.1029/2018gl077670

Escoubet, C., Fehringer, M., and Goldstein, M. (2001). "Introduction: the cluster Mission," in *Annales Geophysicae*, 19. Copernicus Publications Göttingen, Germany, 1197–1200.

Formisano, V., and Hedgecock, P. (1973). Solar wind interaction with the earth's magnetic field: 3. on the earth's bow shock structure. *J. Geophys. Res.* 78, 3745–3760. doi: 10.1029/ja078i019p03745

Fuselier, S. A., Anderson, B. J., Gary, S. P., and Denton, R. E. (1994). Inverse correlations between the ion temperature anisotropy and plasma beta in the earth's quasi-parallel magnetosheath. *J. Geophys. Res. Space Phys.* 99, 14931–14936. doi: 10.1029/94ja00865

Gosling, J., Asbridge, J., Bame, S., Paschmann, G., and Sckopke, N. (1978). Observations of two distinct populations of bow shock ions in the upstream solar wind. *Geophys. Res. Lett.* 5, 957–960. doi: 10.1029/gl005i011p00957

Hartinger, M., Turner, D., Plaschke, F., Angelopoulos, V., and Singer, H. (2013). The role of transient ion foreshock phenomena in driving Pc5 ULF wave activity. *J. Geophys. Res. Space Phys.* 118, 299–312. doi: 10.1029/2012ja018349

Jakosky, B. M., Lin, R. P., Grebowsky, J. M., Luhmann, J. G., Mitchell, D., Beutelschies, G., et al. (2015). The Mars atmosphere and volatile evolution (MAVEN) mission. *Space Sci. Rev.* 195, 3–48. doi: 10.1007/s11214-015-0139-x

Kajdič, P., Pfau-Kempf, Y., Turc, L., Dimmock, A. P., Palmroth, M., Takahashi, K., et al. (2021). ULF wave transmission across collisionless shocks: 2.5 d local hybrid simulations. *J. Geophys. Res. Space Phys.* 126, e2021JA029283. doi: 10.1029/2021ja029283

Kajdič, P., Blanco-Cano, X., Turc, L., Archer, M., Raptis, S., Liu, T. Z., et al. (2024). Transient upstream mesoscale structures: drivers of solar-quiet space weather. *Front. Astronomy Space Sci.* 11, 1436916. doi: 10.3389/fspas.2024.1436916

Kajdič, P., Blanco-Cano, X., Rojas-Castillo, D., and Omidi, N. (2026). Different transient phenomena at the edges of traveling foreshocks. *J. Geophys. Res. Space Phys.* 131, e2025JA034777. doi: 10.1029/2025ja034777

Karlsson, T., Kullen, A., Liljeblad, E., Brenning, N., Nilsson, H., Gunell, H., et al. (2015). On the origin of magnetosheath plasmoids and their relation to magnetosheath jets. *J. Geophys. Res. Space Phys.* 120, 7390–7403. doi: 10.1002/2015ja021487

Karlsson, T., Raptis, S., Trollvik, H., and Nilsson, H. (2021). Classifying the magnetosheath behind the quasi-parallel and quasi-perpendicular bow shock by local measurements. *J. Geophys. Res. Space Phys.* 126, e2021JA029269. doi: 10.1029/2021ja029269

Karlsson, T., Trollvik, H., Raptis, S., Nilsson, H., and Madanian, H. (2022). Solar wind magnetic holes can cross the bow shock and enter the magnetosheath. *Ann. Geophys. Copernic. Publ. Göttingen, Ger.* 40, 687–699. doi: 10.5194/angeo-40-687-2022

King, J. H., and Papitashvili, N. E. (2005). Solar wind spatial scales in and comparisons of hourly Wind and ACE plasma and magnetic field data. *J. Geophys. Res. Space Phys.* 110, A02104. doi: 10.1029/2004JA010649

Koller, F., Raptis, S., Temmer, M., and Karlsson, T. (2024). The effect of fast solar wind on ion distribution downstream of earth's bow shock. *Astrophysical J. Lett.* 964, L5. doi: 10.3847/2041-8213/ad2ddf

Krämer, E., Koller, F., Suni, J., LaMoury, A. T., Pöppelwerth, A., Glebe, G., et al. (2024). Jets downstream of collisionless shocks: recent discoveries and challenges. *Space Sci. Rev.* 221, 4. doi: 10.1007/s11214-024-01129-3

Liu, T. Z., Angelopoulos, V., Dorfman, S., Hartinger, M. D., Zhang, K., Raptis, S., et al. (2025). Statistical relationship between foreshock ULF wave power and ground-based Pc3-4 wave power. *J. Geophys. Res. Space Phys.* 130, e2025JA033760. doi: 10.1029/2025ja033760

Liu, T. Z., Angelopoulos, V., Dorfman, S., Hartinger, M. D., Raptis, S., Zhang, K., et al. (2026). Relationship between magnetosheath ULF waves and ground-based

Pc3-4 waves: a statistical study. *J. Geophys. Res. Space Phys.* 131, e2025JA034763. doi: 10.1029/2025ja034763

Luhmann, J., Russell, C., and Elphic, R. (1986). Spatial distributions of magnetic field fluctuations in the dayside magnetosheath. *J. Geophys. Res. Space Phys.* 91, 1711–1715. doi: 10.1029/ja091ia02p01711

Mailyan, B., Munteanu, C., and Haaland, S. (2008). What is the best method to calculate the solar wind propagation delay? *Ann. geophysicae Copernic. GmbH* 26, 2383–2394. doi: 10.5194/angeo-26-2383-2008

Mohammed-Amin, T., Krämer, E., Nesbit-Östman, S., Gunell, H., and Simon Wedlund, C. (2025). Jets downstream of the martian bow shock: occurrence in the 2014–2024 period. *Astronomy & Astrophysics* 696, A75. doi: 10.1051/0004-6361/202453557

Omidi, N., Berchem, J., Sibeck, D., and Zhang, H. (2016). Impacts of spontaneous hot flow anomalies on the magnetosheath and magnetopause. *J. Geophys. Res. Space Phys.* 121, 3155–3169. doi: 10.1002/2015ja022170

O'Brien, C., Walsh, B. M., Zou, Y., Tasnim, S., Zhang, H., and Sibeck, D. G. (2023). PRIME: a probabilistic neural network approach to solar wind propagation from l1. *Front. Astronomy Space Sci.* 10, 1250779. doi: 10.3389/fspas.2023.1250779

Pecora, F., Chhiber, R., Roy, S., Chasapis, A., Vo, T., Sorriso-Valvo, L., et al. (2026). General properties of the magnetosheath: the mms unbiased campaign. *J. Geophys. Res. Space Phys.* 131, e2025JA034919. doi: 10.1029/2025ja034919

Plaschke, F., Hietala, H., Archer, M., Blanco-Cano, X., Kajdič, P., Karlsson, T., et al. (2018). Jets downstream of collisionless shocks. *Space Sci. Rev.* 214, 81. doi: 10.1007/s11214-018-0516-3

Pollock, C., Moore, T., Jacques, A., Burch, J., Gliese, U., Saito, Y., et al. (2016). Fast plasma investigation for magnetospheric multiscale. *Space Sci. Rev.* 199, 331–406. doi: 10.1007/s11214-016-0245-4

Raptis, S., Aminalragia-Giamini, S., Karlsson, T., and Lindberg, M. (2020a). Classification of magnetosheath jets using neural networks and high resolution OMNI (HRO) data. *Front. Astronomy Space Sci.* 7, 24. doi: 10.3389/fspas.2020.00024

Raptis, S., Karlsson, T., Plaschke, F., Kullen, A., and Lindqvist, P. (2020b). Classifying magnetosheath jets using MMS: statistical properties. *J. Geophys. Res. Space Phys.* 125, e2019JA027754. doi: 10.1029/2019ja027754

Raptis, S., Karlsson, T., Vaivads, A., Pollock, C., Plaschke, F., Johlander, A., et al. (2022). Downstream high-speed plasma jet generation as a direct consequence of shock reformation. *Nat. Commun.* 13, 598. doi: 10.1038/s41467-022-28110-4

Raptis, S., Lindberg, M., Liu, T. Z., Turner, D. L., Lalti, A., Zhou, Y., et al. (2025). Multimission observations of relativistic electrons and high-speed jets linked to shock-generated transients. *Astrophysical J. Lett.* 981, L10. doi: 10.3847/2041-8213/adb154

Retinò, A., Khotyaintsev, Y., Le Contel, O., Marcucci, M. F., Plaschke, F., Vaivads, A., et al. (2022). Particle energization in space plasmas: towards a multi-point, multi-scale plasma observatory. *Exp. Astron.* 54, 427–471. doi: 10.1007/s10686-021-09797-7

Sibeck, D., Lee, S.-H., Omidi, N., and Angelopoulos, V. (2021). Foreshock cavities: direct transmission through the bow shock. *J. Geophys. Res. Space Phys.* 126, e2021JA029201. doi: 10.1029/2021ja029201

Svenningsson, I., Yordanova, E., Khotyaintsev, Y. V., André, M., and Cozzani, G. (2025). Classifying the magnetosheath using local measurements from MMS. *J. Geophys. Res. Space Phys.* 130, e2024JA033272. doi: 10.1029/2024ja033272

Thomas, B. A., Vandegriff, J. D., Antunes, A. K., Bradford, J. W., Yeakel, K., Mo, W., et al. (2022). HelioCloud: a community cloud-based approach to heliophysics analytics and software development. *AGU Fall Meet. Abstr.* 2022 (SH45B–01).

Torbert, R. B., Russell, C. T., Magnes, W., Ergun, R. E., Lindqvist, P.-A., LeContel, O., et al. (2014). The FIELDS instrument suite on MMS: scientific objectives, measurements, and data products. *Space Sci. Rev.* 199, 105–135. doi: 10.1007/s11214-014-0109-8

Toy-Edens, V. (2024). *8 Years of Dayside Magnetospheric Multiscale (MMS) Unsupervised Clustering Plasma Regions Classifications*. doi: 10.5281/ZENODO.10491878

Toy-Edens, V., Mo, W., Raptis, S., and Turner, D. L. (2024). Classifying 8 years of MMS dayside plasma regions *via* unsupervised machine learning. *J. Geophys. Res. Space Phys.* 129, e2024JA032431. doi: 10.1029/2024JA032431

Toy-Edens, V., Mo, W., Allen, R. C., Vines, S. K., and Raptis, S. (2025). Automated classification of MESSENGER plasma observations *via* unsupervised transfer learning. *Front. Astronomy Space Sci.* 12, 1608091. doi: 10.3389/fspas.2025.1608091

Toy-Edens, V., Mo, W., and Raptis, S. (2026). *Shock Detectives: Classifying MMS Observations of Earth's Magnetosheath via Citizen Science - Dataset*. doi: 10.5281/ZENODO.22210989

Trotta, D., Pecora, F., Settino, A., Perrone, D., Hietala, H., Horbury, T., et al. (2022). On the transmission of turbulent structures across the earth's bow shock. *Astrophysical J.* 933, 167. doi: 10.3847/1538-4357/ac7798

Turc, L., Roberts, O. W., Verscharen, D., Dimmock, A. P., Kajdič, P., Palmroth, M., et al. (2022). Transmission of foreshock waves through earth's bow shock. *Nat. Phys.* 19, 78–86. doi: 10.1038/s41567-022-01837-z

Vokhmyanin, M., Stepanov, N., and Sergeev, V. (2019). On the evaluation of data quality in the OMNI interplanetary magnetic field database. *Space weather.* 17, 476–486. doi: 10.1029/2018sw002113

Walsh, B. M., Bhakyapaibul, T., and Zou, Y. (2019). Quantifying the uncertainty of using solar wind measurements for geospace inputs. *J. Geophys. Res. Space Phys.* 124, 3291–3302. doi: 10.1029/2019ja026507

Wang, B., Liu, T., Nishimura, Y., Zhang, H., Hartinger, M., Shi, X., et al. (2020). Global propagation of magnetospheric Pc5 ULF waves driven by foreshock transients. *J. Geophys. Res. Space Phys.* 125, e2020JA028411. doi: 10.1029/2020ja028411

Xirogiannopoulou, N., Goncharov, O., Šafránková, J., and Němeček, Z. (2026). Relationship between foreshock structures and magnetosheath jets. *J. Geophys. Res. Space Phys.* 131, e2026JA035161. doi: 10.1029/2026ja035161

Yordanova, E., Vörös, Z., Raptis, S., and Karlsson, T. (2020). Current sheet statistics in the magnetosheath. *Front. Astronomy Space Sci.* 7, 2. doi: 10.3389/fspas.2020.00002

Zhang, C., Dong, C., Liu, T. Z., Mazelle, C., Raptis, S., Zhou, H., et al. (2025). Role of ULF waves in reforming the Martian bow shock. *AGU Adv.* 6, e2025AV001654. doi: 10.1029/2025av001654

Zhou, Y., Wang, B., Raptis, S., Wang, S., Guo, J., Shue, J., et al. (2026). Reconstructing the geometry of a hot flow anomaly with bounding jets in magnetosheath. *Geophys. Res. Lett.* 53. doi: 10.1029/2025gl119404